



Cite this: *Phys. Chem. Chem. Phys.*,
2019, 21, 800

Influence of glycerol on the cooling effect of pair hydrophobicity in water: relevance to proteins' stabilization at low temperature†

Vikas Dubey  and Snehasis Daschakraborty *

Glycerol, as a cosolvent of water, stabilizes proteins under extreme conditions (both at high and low temperatures). However, the mechanism of stabilization of proteins by glycerol at low temperature is still elusive. Because the decrease of hydrophobic interactions at a lower temperature is one of the crucial factors for the cold denaturation, we ask here whether glycerol protects the hydrophobic interactions upon cooling and thereby acts against cold denaturation. Here, we have performed potential of mean force (PMF) calculations, using the umbrella sampling technique, between a pair of methane hydrophobic solute molecules either in pure water or in binary mixtures of water and glycerol for two different compositions and each of them at four different temperatures. We have found that glycerol increases the pair hydrophobic interaction at all the temperatures studied and that the enhancement is more prominent at the lower temperatures studied here. Decomposition of the PMF into the enthalpic and the entropic components and detailed molecular structural analyses give insight into the above observation. We have found that the enhancement of the hydrophobic interaction with increasing glycerol concentration occurs primarily due to the strengthening of the glycerol–water interaction near the associated methane solute molecule pair and the tetrahedral ordering of the H-bonding network being made uniform around the solute by the added glycerol molecules. These results indirectly justify the efficacy of glycerol for the preservation of proteins against cold denaturation at low temperature.

Received 18th October 2018,
Accepted 4th December 2018

DOI: 10.1039/c8cp06513f

rs.li/pccp

1. Introduction

Glycerol is a versatile solvent having many biological and industrial applications when mixed with water. It has efficacy in protecting living cells and tissues by preventing freezing of both intracellular and extracellular fluid at subzero temperatures.^{1–5} Apart from the above colligative anti-freezing property of glycerol, it can also act as an osmolyte to reduce the loss of cellular water.^{5–7} Strong hydrogen (H-) bonding between glycerol and water is responsible for the water retention and cryoprotection activities of glycerol.^{8–15} Apart from the above properties, glycerol stabilizes

proteins under extreme conditions, like heat stress, cold shock, high pressure, *etc.*^{16–26} It has been observed that glycerol and some other protein stabilizers—*e.g.* trehalose, sucrose *etc.*—increase the thermal denaturation temperature and decrease the cold denaturation temperature of proteins.²¹ Also, the effect of protein stabilizers on cold denaturation temperatures is much more intense than the effect on thermal denaturation temperatures.²¹ Extensive theoretical and computer simulation studies have significantly contributed to the understanding of the general mechanism of protein stabilization by glycerol (and some other sugar molecules) at ambient and higher temperatures.^{19,27–30} Macroscopic thermodynamic calculations indicated that glycerol stabilizes the protein by increasing the free energy of the denatured state more than the free energy of the native state and thereby increases the free energy difference between the two states.^{19,28} This happens due to an unequal preferential exclusion of the cosolvent from the surface of the protein in native and denatured states due to a significant change of the surface area. This thermodynamic justification has been indirectly evidenced in molecular theory and simulation.^{27,29,30}

Despite extensive studies on the stabilization mechanism of proteins by glycerol at higher temperatures, much less attention has been paid so far to the mechanism of protein stabilization

Department of Chemistry, Indian Institute of Technology Patna, Bihar 801106, India. E-mail: snehasis@iitp.ac.in

† Electronic supplementary information (ESI) available: (1) Weighed histogram showing the sufficiency of sampling windows, (2) figures showing the convergence of the PMF, (3) alternate way of presenting PMF curves, (4) decomposition of entropy and enthalpy components of the PMF for $T = 280$ K and 300 K, (5) solvent contribution towards the PMF for $T = 280$ K and 300 K, (6) table showing data of free energy, entropy and enthalpy at different minima of the PMF, (7) the RDF between methane solute C and solvent water O_w in pure water at four different temperatures, (8) the RDF between the methane solute and solvent molecules at $T = 280$ K and 300 K, and (9) the number of H-bonds per solvent water molecule as a function of methane–methane separation for pure water at three different temperatures. See DOI: 10.1039/c8cp06513f

by glycerol against cold denaturation. Recent times have witnessed an intense debate on the possible explanation for the observed cold denaturation of proteins. While thermal denaturation is much more straightforward, the origin of cold denaturation is still elusive. Denaturation of proteins at high temperature is generally explained in the following two ways.^{31–39} (1) A large kinetic energy value of the system at high temperature leads to a large fluctuation of the tertiary structure of the protein. (2) The thermal denaturation can also be explained from a thermodynamic perspective. For the folded (F) \rightarrow unfolded (U) transformation of proteins, one can write the standard Gibbs free energy for the transformation as $\Delta G_{F \rightarrow U} = \Delta H_{F \rightarrow U} - T\Delta S_{F \rightarrow U}$. Here, $\Delta G_{F \rightarrow U}$, $\Delta H_{F \rightarrow U}$, and $\Delta S_{F \rightarrow U}$ are the changes of the Gibbs free energy, the enthalpy, and the entropy for the F \rightarrow U transformation. T is the temperature. It is generally observed that both $\Delta H_{F \rightarrow U}$ and $\Delta S_{F \rightarrow U}$ are positive during thermal denaturation occurrence. Therefore $\Delta G_{F \rightarrow U}$ decreases with increasing temperature. This makes the denaturation process more and more thermodynamically favorable. Above a certain temperature, when the entropy component dominates over the enthalpy component, $\Delta G_{F \rightarrow U}$ becomes negative. Therefore, above that temperature protein unfolding becomes spontaneous and thus the protein denatures.

Unlike thermal denaturation, the origin of cold denaturation of proteins is not fully understood. Following are some views existing in the literature. (1) The majority of experimental and computer simulation studies have suggested that the reduction of the hydrophobic interactions, which hold the tertiary structure of the protein together, due to lowering of temperature is the driving force for cold denaturation.^{40–57} (2) Some other simulation studies suggested that the increasing interaction between the hydrophilic residues of the protein and water with decreasing temperature is mainly responsible for unfolding the tertiary structure of the protein.^{58,59} (3) A Monte Carlo simulation study found strong evidence that increasing water–water H-bonding at the protein interface with lowering temperature is a necessary and sufficient condition for the protein's cold denaturation.⁶⁰

The above explanations for cold denaturation of proteins set the stage for exploring the possible roles of glycerol in preserving proteins' structure and functionality at low temperature on a fundamental level. It is possible that glycerol effectively reduces the impact of the above three factors of cold denaturation and thereby preserves the structure and function of a protein at low temperature. In a recent paper, one of us has focused on how glycerol and DMSO disrupt the H-bonding and tetrahedral structure of solvent water around a model hydrophobic solute at subzero temperatures.¹¹ The above study implicitly addressed that the similar disruption of the hydration structure near a protein's hydrophobic core by glycerol or DMSO could effectively assist in preserving the protein's structure at low temperature.

In the present work, our primary goal is to see how glycerol influences the pair hydrophobicity of two simple nonpolar solute molecules in water and whether the hydrophobic interaction is somewhat retained against the observed reduction at a lower temperature.⁵³ This is motivated by earlier observations that the reduction of the hydrophobic interactions in water at a lower temperature is the key factor for cold denaturation if

glycerol were capable of stabilizing the hydrophobic moiety at a lower temperature. A number of studies have already focused on how different protein stabilizers affect the pair hydrophobic interaction between two nonpolar solute molecules in water at ambient or higher temperatures.^{61–72} It was observed that with increasing concentration of trehalose—a well-known protein stabilizer—in water the dispersion of neopentane hydrophobic solute molecules increases.^{61,62} It was argued that trehalose decreases the neopentane–neopentane association constant value by reducing the hydrophobic interaction between them.^{61,62} A separate study, addressing the effect of trimethylamine *N*-oxide (TMAO) on pair hydrophobicity, did not see any role of TMAO.⁶⁴ The above inert behavior of TMAO towards hydrophobicity was thought to be the reason why TMAO is a good osmolyte. However, it has been recently found that upon addition of TMAO to water the large favorable entropic contribution and the unfavorable enthalpy, which are characteristic of hydrophobic interactions, decrease.⁶³ These changes account for the strengthening of hydrophobic interactions when a particular force field model of TMAO is considered. A molecular dynamics (MD) simulation study,⁷⁰ addressing the effect of dimethyl sulphoxide (DMSO) concentration on pair hydrophobicity, observed the following. The pair hydrophobic interaction between two nonpolar solute molecules—measured by the depth of the first free energy minimum—increases with increasing DMSO concentration in water in the lower DMSO concentration regime.⁷⁰ Similar enhancement of pair hydrophobicity has recently been reported with increasing ethanol concentration in water up to a mole fraction of 0.10.⁷¹ It has also been found, in a separate theoretical study, that the direct interaction between cosolvent molecules and nonpolar solute molecules can strengthen hydrophobic interactions and can contribute to stabilizing collapsed globular structures.⁶⁷ In addition to the importance of the above work in understanding the fundamental role of different protein stabilizing agents in influencing hydrophobic interactions in water, these studies connect their findings with the stability issues of proteins in the presence of the above additives.

The above studies have significantly contributed to the understanding of how a cosolvent does affect the pair hydrophobic interaction in water either at ambient or at higher temperatures. Unfortunately, the effect of those substances on pair hydrophobic interactions at lower temperatures is not much explored, despite its huge application in understanding the action of different protein stabilizers against cold denaturation at low temperature. Retention of hydrophobic interactions at low temperature can effectively prevent cold denaturation of the protein. Therefore, we study here the effect of glycerol on the pair hydrophobic interaction between two methane molecules (a small hydrophobic solute) for a wide range of temperatures. We have calculated the PMF between a pair of methane hydrophobic solute molecules using the umbrella-sampling method in all-atom MD simulations at different temperatures and compositions of the binary solvent mixture of water and glycerol.

The outline for the remainder of this paper is as follows. The molecular models and other simulation details are detailed

in Section 2. Section 3 presents the simulation results and discussion. Concluding remarks are offered in Section 4.

2. Method

2.1 Simulation details

All simulations are performed using the GROMACS package.⁷³ Our simulation box contains a pair of methane molecules dissolved in 2000 solvent molecules. The solvent is either pure water or binary mixtures of glycerol and water with mole fractions of glycerol $x_G = 0.05$ or 0.1 . For each of the three compositions, we have considered four different temperatures, $T = 260$ K, 280 K, 300 K, and 320 K. Due to the fact that the freezing point of the TIP4P/2005 water model (the force field model we have used in the present work) is 252 K at atmospheric pressure, we have not chosen a temperature below 260 K. In addition, on further lowering of the temperature below 260 K, the glycerol/water mixture (even at $x_G = 0.1$) becomes highly viscous and the dynamics become much slower. Therefore, the PMF results are expected to be erroneous and hence inconclusive. The rationale of choosing the highest mole fraction of glycerol as 0.1 (equivalent to a 0.36 weight fraction or 4.45 M concentration of glycerol) is as follows. This binary mixture composition has sufficient cryoprotecting ability as the freezing point of the mixture decreases by 20 degrees.⁷⁴ Also, this composition of the glycerol/water mixture was already seen to have efficacy in thermal stabilization of proteins.^{21,27–30} It is worth mentioning that a past experiment observed that the cold denaturation temperature of a protein can be decreased by 35 degrees at sucrose concentrations (another polyol having strong protein stabilizing activity) as low as 0.9 M.²¹

All-atom modeling of a glycerol molecule is done by force field parameters that were developed and modified by Chelli *et al.*⁷⁵ and Blicek *et al.*,⁷⁶ respectively. Water molecules are modeled by the TIP4P/2005 force field,⁷⁷ the most efficient model of water at all temperatures including the deeply supercooled region. (More popular models of water, like SPC/E *etc.*, are not appropriate as these models do not provide a good prediction of various microscopic and thermodynamic properties specifically at subzero temperatures.) The above combination of the force field models of water and glycerol has proven efficacy in reproducing various thermodynamic, microscopic structural and dynamical properties for a wide range of temperatures including sub-zero.⁷⁸ Methane is modeled using OPLS/AA force field parameters.⁷⁹

The equation of motion is solved every 2 fs using the leap-frog algorithm. Long-range electrostatic interactions are handled by the particle mesh Ewald summation technique. We first equilibrate the system for a 50 ns simulation time using the isobaric-isothermal (*NPT*) ensemble. The No -Hoover thermostat^{80,81} is used for maintaining the system at a constant temperature. The pressure is kept constant by the use of the Parrinello–Rahman barostat.⁸² A coupling time of 0.5 ps is set for both the thermostat and the barostat.

The PMF has been calculated using the umbrella sampling method.⁸³ We vary the separation between the pair of methane

solute molecules from 0.3 nm to 1.3 nm with a gap of 0.1 nm, resulting in a total of 11 different simulation systems for a particular temperature and composition of the glycerol/water mixture. This aggregates to a total of 132 simulation systems with varying temperature and composition of the solvent mixture. For each of the systems, we obtain the initial configuration with the desired distance between the two methane solute molecules using the pull code in GROMACS. Such a small interval is chosen to ensure sufficient overlap between two neighboring windows. Fig. S1 of the ESI† presents a representative figure, which shows the overlap between the neighboring windows. Long simulations are performed starting from the above initial configurations with the distance between the methane molecules restrained by a harmonic potential with a force constant of 1000 kJ mol^{−1} nm^{−2}. Each configuration is simulated for a long time (50 ns for pure water and 100 ns for the two binary mixtures having $x_G = 0.05$ and 0.1) to get sufficient sample points. This aggregates to a total of 11.6 μ s simulation time. The first 5 ns is not considered for calculating the PMF. The weighed histogram analysis method (WHAM)⁸⁴ at each window has been used to obtain the PMF as a function of the separation between the two methane solute molecules.

We have shown the convergence of the PMF for $x_G = 0.1$ at $T = 260$ K in Fig. S2 and S3 of the ESI.† Fig. S2 (ESI†) plots PMFs, which are calculated from trajectories of increasing length. We clearly see the convergence for trajectories having a duration of more than 50 ns. We have also plotted, in Fig. S3 of the ESI,† the PMF arising from the first 50 ns of the trajectory compared with the PMF obtained from the last 50 ns of the trajectory. The convergence is absolutely clear in the above figures.

We decompose the PMF into enthalpic $H(r)$ and entropic terms $S(r)$ using the finite difference (FD) method.^{53,71,85–88} In this method, the entropy of association is obtained from the temperature derivative of the PMF at each separation (r) between the two methane solute molecules.

$$-S(r) = \frac{G(r, T + \Delta T) - G(r, T)}{\Delta T} \quad (1)$$

The FD method is a widely used technique for obtaining the entropy contribution of the PMF with respect to temperature. It was found that the FD approach performs similar to or better than other alternative methods, like thermodynamic integration, free energy perturbation, *etc.*^{89–91} Despite the great performance of the FD approach there are limitations too. In order to ensure a statistically meaningful estimation of entropy, due to large fluctuations in the complex systems one requires a large temperature gap (ΔT) between simulation systems under the assumption of constant heat capacity. Although the assumption is generally good, the FD approximation breaks down if ΔT is too large. Usually, ΔT is chosen as 20 K. In order to increase the accuracy, a large sampling of data is generally desirable. In this work, we have done enough sampling in terms of the length of the individual trajectories. Our trajectory lengths have a maximum of up to 100 ns, which is much longer than generally collected. Good convergence of the PMF plots, shown in Fig. S2 and S3 of the ESI,† is direct proof of the above claim.

In the present study, we chose ΔT to be 20 K. The enthalpy contribution to the free energy $H(r)$ at temperature T is estimated by the following equation,

$$H(r) = G(r) + TS(r). \quad (2)$$

The solvent contribution, $W_{\text{solv}}(r)$, to the PMF is calculated by subtracting the solute–solute interaction energy $U_{\text{sol-sol}}(r)$ from the total PMF values at different r using the following equation

$$W_{\text{solv}}(r) = G(r) - U_{\text{sol-sol}}(r). \quad (3)$$

$W_{\text{solv}}(r)$ can be decomposed into the entropic $S_{\text{solv}}(r)$ and the enthalpic $H_{\text{solv}}(r)$ terms. While $S_{\text{solv}}(r)$ is actually identical to the total entropy,⁹²

$$S_{\text{solv}}(r) = S(r), \quad (4)$$

the enthalpy from the solvent contribution, $H_{\text{solv}}(r)$, is calculated by subtracting the solute–solute interaction in a vacuum, $U_{\text{sol-sol}}(r)$, from the total enthalpy of association, $H(r)$, using the following equation:

$$H_{\text{solv}}(r) = H(r) - U_{\text{sol-sol}}(r). \quad (5)$$

$H_{\text{solv}}(r)$ is further decomposed into two components: one is due to the solute–solvent interaction $H_{\text{sol-solv}}(r)$ and the remaining part, $H_{\text{rem}}(r)$, captures the change in solvent–solvent interactions as well as the mechanical pressure–volume ($P\Delta V$) work. $H_{\text{sol-solv}}(r)$ is calculated directly from simulation, while $H_{\text{rem}}(r)$ is obtained by subtracting $H_{\text{sol-solv}}(r)$ from $H_{\text{solv}}(r)$

$$H_{\text{rem}}(r) = H_{\text{solv}}(r) - H_{\text{sol-solv}}(r). \quad (6)$$

3. Results and discussion

3.1 Effect of glycerol on the hydrophobic interaction at different temperatures

First, we see how glycerol influences the pair hydrophobic interaction between two methane solute molecules at the different temperatures considered here. We plot, in Fig. 1, the PMFs between the pair of methane molecules either in pure water or in the glycerol/water binary mixture, varying the composition ($x_G = 0.05$, and 0.10) and temperature ($T = 320$ K, 300 K, 280 K, and 260 K) of the system. The following is the procedure by which we put the PMFs on one another in order to do comparative analysis. First, we obtain the PMF using the WHAM analysis technique. Then, we set the PMF to zero at $r = 1.3$ nm. We correct the entropic contribution to the PMF due to rotation of the solute molecules by adding the term $2k_B T \ln(r)$ to the PMF. The uncertainty in the PMF was computed by bootstrap analysis. An alternative presentation of the PMF has also been shown in Fig. S4 of the ESI†

Now we go back to the analysis of Fig. 1. Each PMF shows three minima. The first one, situated at methane–methane separation $r \sim 0.4$ nm, is the contact minimum (CM). The second and the third minima occur approximately at $r \sim 0.7$ nm and ~ 1 nm separations, respectively. The second minimum is the first solvent separated minimum (FSSM)^{53,71,93–97} as only one solvent water layer can fit at this methane–methane separation.

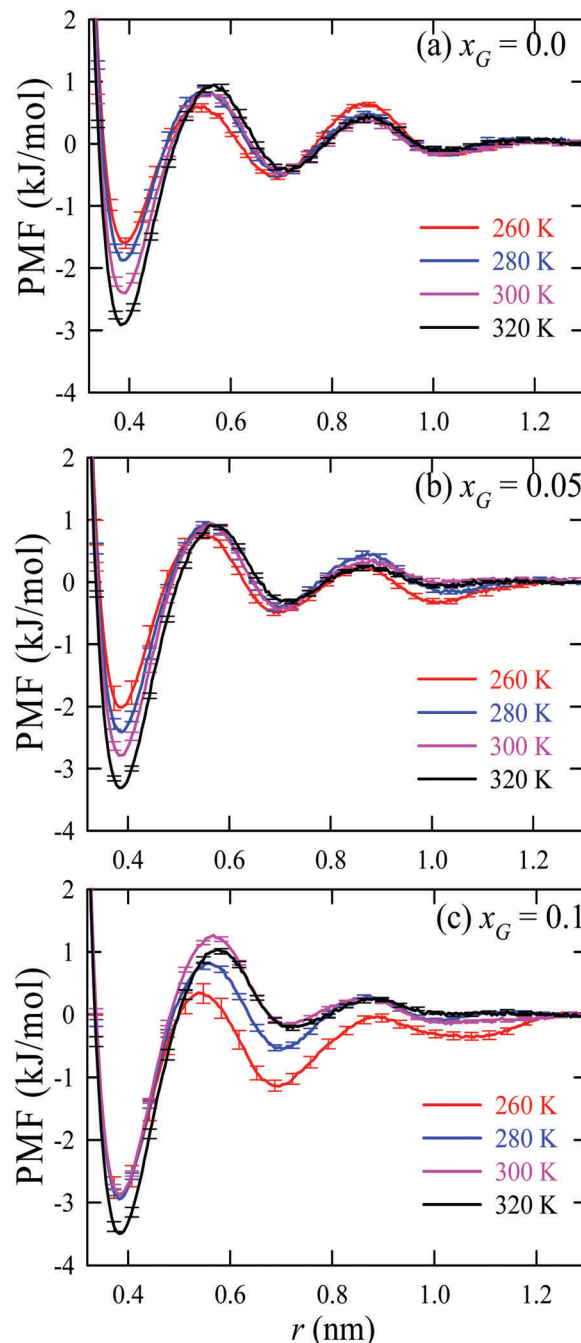


Fig. 1 PMF as a function of the distance between the pair of methane molecules, dissolved either in pure water or in the glycerol/water binary mixture, varying the composition ($x_G = 0.05$, and 0.10), each at 4 different temperatures ($T = 320$ K, 300 K, 280 K, and 260 K).

Similarly, two water solvent layers can comfortably fit inside an $r \sim 1$ nm separation between the two methane molecules. Therefore, the third minimum at $r \sim 1$ nm is also called the second solvent separated minimum (SSSM).^{53,71,93–97} Table S1 of the ESI† lists the depths of the above three minima for systems with differing temperature and solvent composition.

It is clear from Fig. 1a and Table S1 of the ESI† that for pure water at a 300 K temperature the depth of the CM and the FSSM are ~ 2.4 kJ mol⁻¹ and ~ 0.5 kJ mol⁻¹ respectively.

At $r \sim 0.54$ nm—in between the CM and FSSM—there exists the desolvation barrier with a height of ~ 3.2 kJ mol⁻¹. The SSSM is rather a very shallow well with a depth of only ~ 0.2 kJ mol⁻¹. The SSSM is separated from the FSSM by the second barrier, occurring at $r \sim 0.85$ nm, with a height of ~ 0.9 kJ mol⁻¹. All the above numerical values are in good agreement with earlier studies.^{53,93–97} Now, as we decrease the temperature of the system from 320 K to 260 K, the well-depth of the CM reduces from ~ 3.0 kJ mol⁻¹ to ~ 1.6 kJ mol⁻¹. The desolvation barrier height also decreases from ~ 4 kJ mol⁻¹ to ~ 2.2 kJ mol⁻¹. This indicates a significant reduction of the pair hydrophobicity of methane in water with decreasing the temperature. This is consistent with an earlier temperature dependence study.⁵³ However, very subtle changes are noticed in the depths of the FSSM and SSSM, and the height of the second free energy barrier. Similar changes in the depth of the CM and the height of the barrier are observed for the methane–methane PMF in a binary mixture of glycerol and water with glycerol's mole fraction $x_G = 0.05$. Interestingly, for $x_G = 0.10$, the CM well depth is much less sensitive towards the temperature.

The effect of glycerol concentration on the depth of the CM and the height of the desolvation barrier at all the four temperatures is shown in Fig. 2. It is evident from Fig. 2a that the depth of the CM decreases almost linearly with decreasing the temperature for pure water and for the glycerol/water binary mixture for $x_G = 0.05$. However, for $x_G = 0.10$, the depth of the

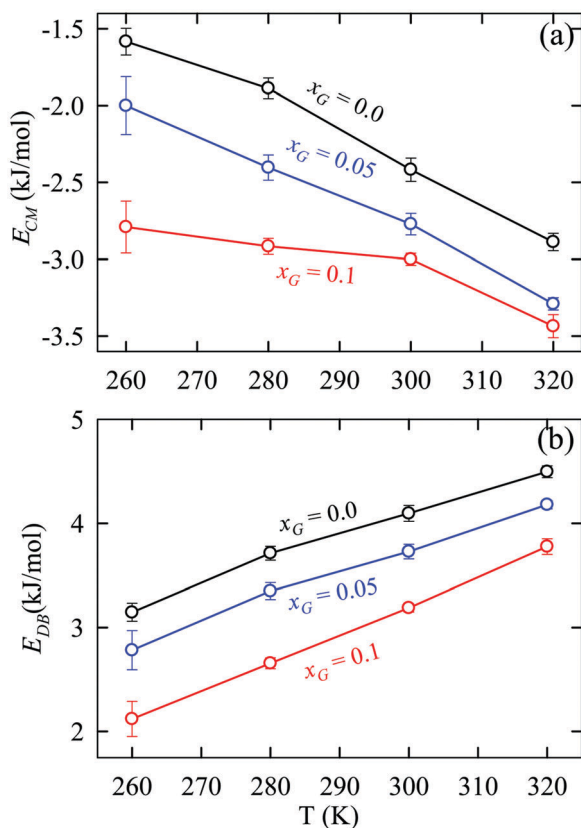


Fig. 2 Temperature dependence of (a) CM well depths and (b) the desolvation barrier height for three different solvent compositions.

CM does not change appreciably below 280 K. With increasing glycerol concentration in the mixture, the depth of the CM increases at all the temperatures studied here. The increase is much more prominent at lower temperatures than at the higher ones. For instance, while the depth of the CM increases from ~ 3 kJ mol⁻¹ (pure water) to ~ 3.5 kJ mol⁻¹ upon increasing x_G from 0.0 to 0.1 at $T = 320$ K, the same increase of glycerol concentration increases the depth of the CM from ~ 1.6 kJ mol⁻¹ to ~ 2.8 kJ mol⁻¹ at $T = 260$ K. This indicates that glycerol is effective for increasing the pair hydrophobicity between the pair of methane molecules at all temperatures and that the efficiency significantly increases at lower temperatures. This might be a molecular level explanation for the experimental observation that glycerol prevents cold denaturation more strongly than thermal denaturation of proteins.²¹ In addition, it is evident from Fig. 2b that glycerol increases the desolvation barrier height at all the temperatures almost uniformly. In addition, Table S1 (ESI†) clearly shows that the free energy difference between the CM and the FSSM increases with increasing the glycerol concentration in the medium. This further supports the fact that dissociation of two small hydrophobic solute molecules becomes unfavorable as the glycerol concentration increases in the medium. This gives a clear signature about the strong efficacy of glycerol in retaining the pair hydrophobic interaction between two hydrophobic molecules in water. From the above observation, one can conjecture a fundamental mechanism of protein stabilization by glycerol at low temperature by retaining the hydrophobic core of proteins in supercooled water. The above results also corroborate with the fact that glycerol is a kosmotrope and therefore increases the hydrophobic interaction between two nonpolar solute molecules in liquid water.⁹⁸

3.2 Decomposition of the PMF into enthalpy and entropy

In order to comprehend the above results on a more fundamental level, we decompose the PMFs into the entropy ($-TS$) and the enthalpy (H) contributions using eqn (1) and (2) respectively. In the present study, we choose $\Delta T = 20$ K in eqn (1) and hence the decomposition of the PMF can be done only at three temperatures, 260 K, 280 K, and 300 K.

Fig. 3 plots the PMF and two components (H and $-TS$) as functions of methane–methane separation r for three different solvent compositions at a 260 K temperature. The above results for 280 K and 300 K temperatures are presented in Fig. S5 and S6 of the ESI† respectively. Table S1 of the ESI† lists the numerical values of H and $-TS$ at the separations of the three minima of the PMF. At the CM separation, $-TS$ is negative but H is positive at all the temperatures for pure water. Therefore, the hydrophobic association of the two methane solute molecules, to form the contact pair, is entropically favorable but enthalpically unfavorable. On the other hand, $-TS$ is positive but H is negative both at the FSSM and the SSSM separations. Therefore, both the above minima of the PMF are enthalpically favorable but entropically unfavorable. This is consistent with earlier studies.^{53,63,71,85–88,92,93}

Now, as glycerol is added to water, both the entropy and enthalpy decrease at the CM separation. A similar observation was reported in recent work on hydrophobicity between two

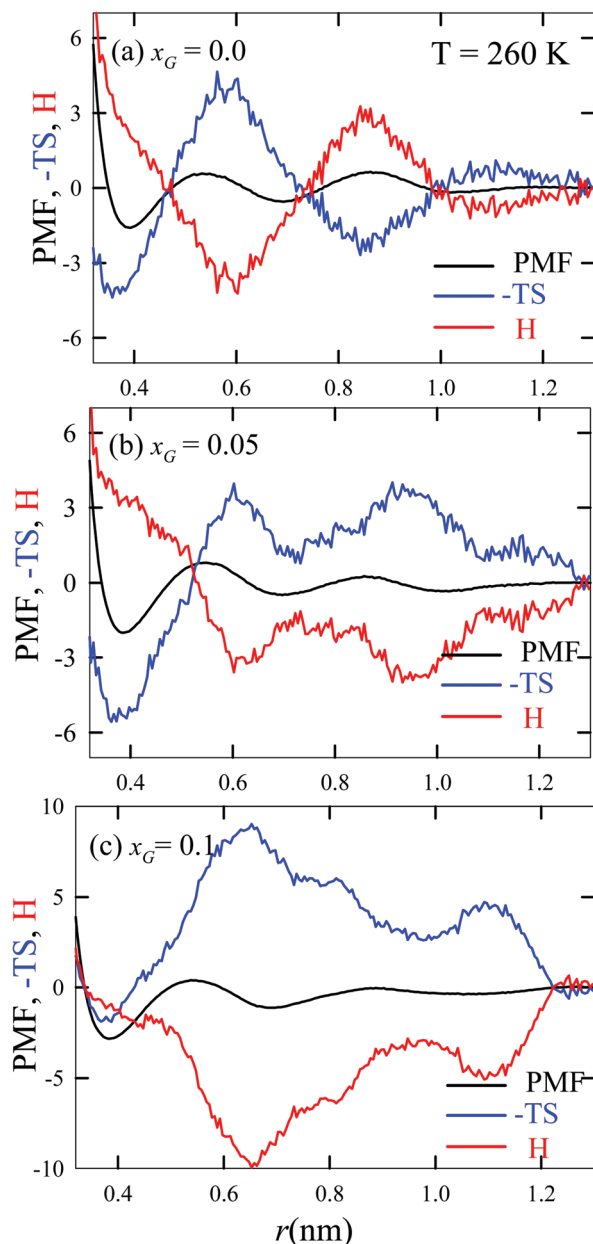


Fig. 3 PMF between the pair of methane solute molecules and its two components, entropy ($-TS$) and enthalpy (H), in (a) pure water, and water/glycerol mixtures with (b) $x_G = 0.05$, and (c) $x_G = 0.1$ at a 260 K temperature.

neopentane molecules in a TMAO/water binary solvent mixture.⁷² While $-TS$ becomes less negative, the positive value of H decreases. For $x_G = 0.1$, both $-TS$ and H become negative at the CM for $T = 280$ K and 260 K temperatures. Therefore, the CM of the PMF is favored both by the enthalpic and the entropic contributions. The above analysis implies that the observed enhancement of the pair hydrophobic interaction, particularly at the lower temperature, is due to the decrease of enthalpy with the increase of glycerol concentration. Fig. 3 and Table S1 (ESI[†]) clearly show that at a 300 K temperature, the addition of glycerol to water decreases the enthalpy of the CM and increases the value of $-TS$. As seen in Fig. S5 and S6 of the

ESI[†], the above changes are much more prominent for the lower temperatures. In addition, the decrease of H is slightly more than that of $-TS$. These uneven changes of the enthalpic and the entropic components result in the overall increase of the CM well depth with increasing glycerol concentration.

To elucidate further, we calculate the solvent contribution to the PMF, W_{solv} , and decompose the same into the enthalpic (H_{solv}) and the entropic ($-TS_{\text{solv}}$) contributions using eqn (3)–(5). They are presented in Fig. 4 for $T = 260$ K and in Fig. S7 and S8 of the ESI[†] for $T = 280$ K and 300 K respectively. As expected, W_{solv} is also negative both at the CM and the FSSM separation at all conditions. At the CM, W_{solv} decreases with decreasing temperature. This is due to the decrease of both the entropic $-TS_{\text{solv}}$ and the enthalpic H_{solv} components at the CM. H_{solv} has contributions from methane solute–solvent ($H_{\text{sol-solv}}$) and solvent–solvent interaction potentials and pressure–volume work ($P\Delta V$). We calculated $H_{\text{sol-solv}}$ (directly from simulation) as a function of r . We set $H_{\text{sol-solv}} = 0$ at an $r = 1.3$ nm separation and then subtract $H_{\text{sol-solv}}$ from H_{solv} to get the remaining enthalpic contribution, H_{rem} .

H_{solv} and its two components $H_{\text{sol-solv}}$ and H_{rem} are plotted as functions of r in Fig. 4d for $T = 260$ K. In all the situations, $H_{\text{sol-solv}}$ is positive at the CM separation and decreases steadily with r . This indicates that the methane–methane contact pair formation is disfavored by $H_{\text{sol-solv}}$. H_{rem} , which has contributions from the solvent–solvent interaction and $P\Delta V$ work, makes a more than 60% contribution to H_{solv} at the CM for pure water. H_{rem} decreases with decreasing the temperature. This could be because of the strengthening of the water solvent–solvent interaction near the hydrophobic solute.^{11,99–108}

Now, we discuss the effect of glycerol on the above components. Fig. 4 presents W_{solv} , H_{solv} , $-TS$, $H_{\text{sol-solv}}$, and H_{rem} as functions of r for different solvent compositions for a 260 K temperature. (See Fig. S7 and S8 of the ESI[†] for the results at the two other temperatures.) Similar to the PMF, W_{solv} also increases with increasing glycerol concentration at the CM at all the temperatures studied here. The decomposition of W_{solv} into the enthalpic and the entropic terms clearly shows that the decrease of W_{solv} at the CM separation arises from the decrease of H_{solv} , which is again caused by the drop of H_{rem} for higher glycerol concentration. We will see in the next subsection that the above decrease of H_{rem} is a direct consequence of the local solvent structure augmentation around the hydrophobic solute in presence of the glycerol cosolvent in water.

3.3 Analysis of the solvent structure around the solute

In this section, we discuss how glycerol influences the solvation structure around the methane hydrophobic solute and thereby explain the observations of the preceding sections from a more fundamental perspective.

Tetrahedral order parameter. We calculate the tetrahedral order parameter q for the solvent molecules separately at the interface and in the bulk using the following equation:^{109,110}

$$q = 1 - \frac{3}{8} \sum_{j=1}^3 \sum_{k=j+1}^4 \left(\cos \theta_{jk} + \frac{1}{3} \right)^2 \quad (7)$$

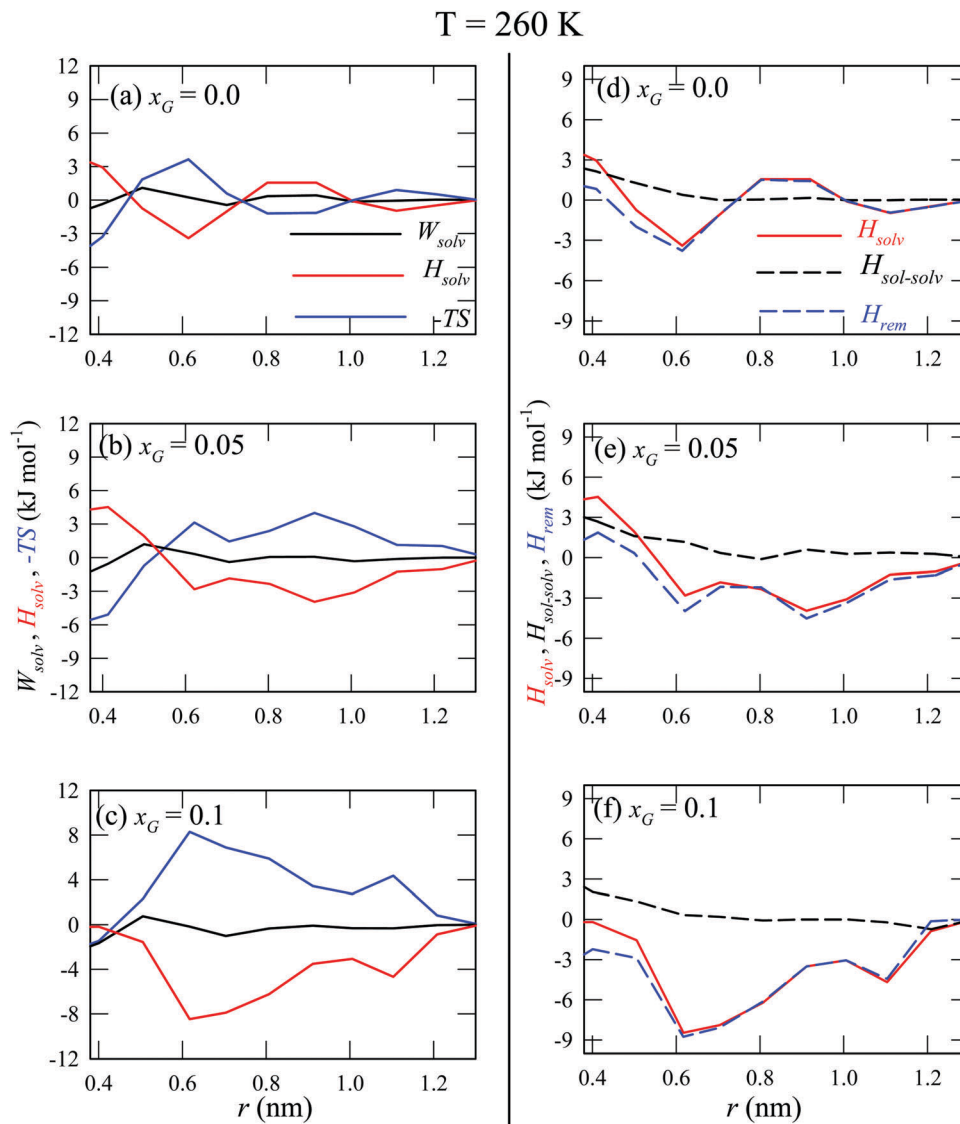


Fig. 4 Solvent contribution of the PMF, W_{solv} , and its two components (entropy ($-TS$) and enthalpy (H_{solv})) as functions of methane–methane separation r in solvent with three different compositions: (a) $x_G = 0.0$, (b) $x_G = 0.05$, and (c) $x_G = 0.1$ at a $T = 280$ K temperature. H_{solv} and its two components, $H_{\text{sol-solv}}$ and H_{rem} , at various r values for (d) $x_G = 0.0$ (e) $x_G = 0.05$, and (f) $x_G = 0.1$ at a 260 K temperature.

Fig. 5 exhibits the distributions of q ($p(q)$) for three different solvent systems, each at three different temperatures, 300 K, 280 K, and 260 K. q has been calculated for the solvent molecules (both water and glycerol) around a central water molecule, which is either at the interface or in the bulk region. Note that the interface (up to $r \sim 5.5$ Å) and the bulk (outside the distance $r \sim 11$ Å) are identified by the radial distribution function (RDF) between the methane solute and solvent water, presented in Fig. S9 of the ESI.† Fig. 5 clearly shows that $p(q)$ has a maximum at $q \sim 0.83$ and a shoulder at $q \sim 0.50$ under all conditions. While the peak at $q \sim 0.83$ corresponds to an almost perfect tetrahedral structure, the shoulder at $q \sim 0.50$ corresponds to the trigonal pyramidal geometry of water molecules with missing water from one vertex of the tetrahedron.¹¹

A closer inspection of Fig. 5 further reveals that $p(q)$ for interfacial water molecules has a slightly more intense peak at

$q \sim 0.83$ than that for the bulk water molecules. This is prominent for the pure water case. Therefore, the interfacial water molecules are more tetrahedrally ordered than the bulk ones at all the temperatures studied for $x_G = 0.0$. This is popularly known as hydrophobic iceberg formation of water adjacent to a hydrophobe.^{99–108} So, when two hydrophobic solute molecules approach towards each other to form a contact pair, some water molecules are released from the interface due to the excluded volume effect. Now, as we add glycerol to water, both the interfacial and the bulk solvent become less tetrahedral. This is common for all the temperatures studied. This indicates that the added glycerol molecules decrease the tetrahedral order of water both at the hydrophobic solute interface and in the bulk. A closer view of Fig. 5 further reveals that $p(q)$ for the interfacial water closely resembles that of the bulk water at a 0.1 mole fraction of glycerol. This suggests that glycerol

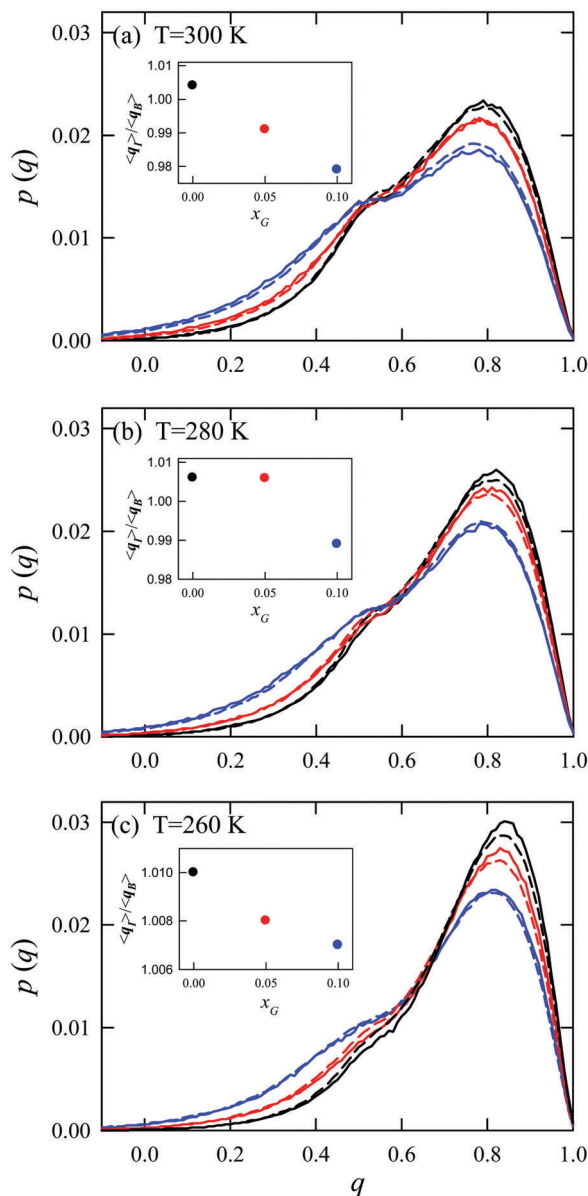


Fig. 5 Glycerol concentration dependence of the distribution of tetrahedral order parameter q for interfacial (solid line) and bulk (dashed line) solvent with different compositions: $x_G = 0.0$ (black), $x_G = 0.05$ (red), and $x_G = 0.10$ (blue) at three temperatures (a) $T = 300$ K, (b) $T = 280$ K, (c) $T = 260$ K. The ratio of averaged q between the interfacial and the bulk solvent, $\langle q_I \rangle / \langle q_B \rangle$, at each temperatures is shown in the inset as a function of x_G .

symmetrizes the tetrahedral ordering of the solvent across space around the hydrophobic solute and that directly impacts the increasing entropy for contact pair formation. The water molecules, released from the interface, do not increase the overall entropy of the system. This explains the decreasing value of $-TS$ at the CM with increasing glycerol concentration.

Radial distribution function. Now, we turn our focus to explaining the reason for decreasing enthalpy H at the CM with increasing glycerol concentration. Fig. 6 shows the RDF between the methane solute and solvent molecules at $T = 260$ K as a representative temperature for three different solvent

compositions. (The pictures for the other two temperatures are presented in Fig. S10 and S11 of the ESI†) Fig. 6a clearly shows that for pure water the first peak intensity decreases as the solute pair molecules approach closer to each other. This reduction of the first peak intensity of the RDF confirms the exclusion of some solvent water molecules from the interface because of the reduced volume of the interfacial layer. The above exclusion of water molecules from the interface—due to the hydrophobic association of the two methane solute molecules—results in an overall loss of H-bond strength. (The H-bond number per solvent water molecule is plotted, in Fig. S12 of the ESI,† as a function of distance from the solute.) Therefore, the hydrophobic association leads to an increase of the enthalpy of the system and the association becomes an enthalpy-disfavored process. Therefore, the exclusion of the interfacial water molecules due to the association of the hydrophobes actually results in an increase of enthalpy.

Fig. 6b and c suggest that the decrease of the first peak intensity of the methane–water RDF, as discussed in the above paragraph, is almost insensitive to the glycerol concentration. However, the RDF between methane and glycerol molecules is something interesting. Here, the first peak intensity increases slightly as two methane solute molecules form a contact pair starting from the dissociated state. This suggests that the reduction of the interfacial solvation shell width (due to the association of the solute pair) does not affect the coordination number of glycerol molecules around the methane solute. Therefore, the hydrophobic association process triggers the inclusion of glycerol molecules from the bulk. This can be explained using the preferential interaction of glycerol with the methane solute *via* the hydrophobic interaction between them.¹¹ The inclusion of glycerol molecules in the interfacial layer, when two methane solute molecules aggregate together to form a contact pair, must increase the glycerol–glycerol and glycerol–water interactions and thereby decreases the enthalpy at the CM.

4. Conclusion

Here, we have systematically studied the effect of glycerol on pair hydrophobicity in water at different temperatures ranging from 320 K to 260 K using the umbrella sampling technique in all-atom MD simulations. The PMF has been calculated at different separations of the methane solute pair. Addition of glycerol to water increases the well-depth of the CM of the PMF between the pair of methane solute molecules at all the temperatures studied. The desolvation barrier between the CM and FSSM also increases with glycerol's concentration. The above action of glycerol is more prominent at a lower temperature than that at the higher ones. This shows that glycerol has greater efficacy in preserving the hydrophobic interaction at a lower temperature, which otherwise decreases with decreasing temperature of the medium. This result has an important implication in understanding the mechanism of stabilization of proteins at low temperature by preventing cold

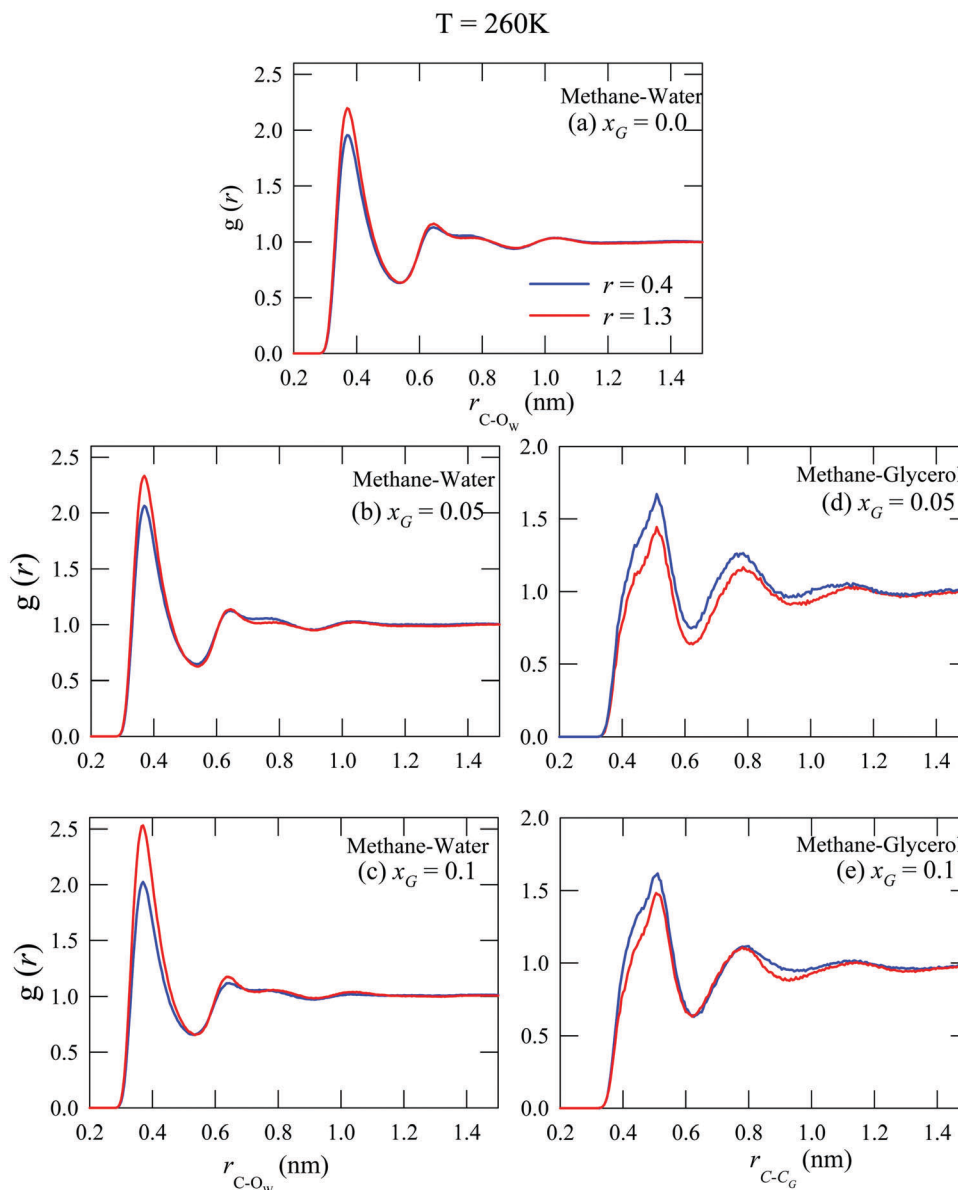


Fig. 6 Radial distribution functions between the methane solute (C atom) and the solvent molecules (water's O_w and glycerol's C_G atom) for three different solvent compositions $x_G = 0.0, 0.05,$ and $0.1,$ at $T = 260$ K.

denaturation, which is supposed to occur *via* reduction of hydrophobic interactions at a lower temperature.^{40–56}

In order to obtain further insight, we have separated out the enthalpic (H) and the entropic ($-TS$) contributions of the PMF by the FD method. From these analyses, we have understood that at the separation of the CM, $-TS$ increases and H decreases with increasing glycerol concentration. However, the above changes are not exactly the same as each other. The larger decrease of H than the increase of $-TS$ ultimately increases the CM well depth of the PMF with an increase of glycerol concentration. Further analyses of various components of H terms and more detailed solvation analyses show that the reduction of the H value at the CM separation originally comes from the increase of the solvent-solute interaction near the hydrophobic solute molecules as they aggregate together to form a contact pair. In addition, glycerol

induces symmetrization of the tetrahedral ordering of the solvent across the space surrounding the hydrophobic solute. The above symmetrization causes a reduction of the entropy contribution of the PMF at the CM separation.

Lastly, one can question the transferability of the findings of the present study to a more complex system, like a protein. The question is pertinent because our choice of the nonpolar solute, methane, is different from a protein, which is bigger and much more complex. A number of studies (see for example, ref. 64 and 111–117) extensively studied the solute length scale dependence of hydrophobic hydration. Drying of the extended nonpolar surface was observed once the size of a hydrophobic solute goes beyond a certain length scale (1 nm size).¹¹¹ Interestingly, the small-to-large crossover length scale can be varied by different means, like the addition of some cosolvents. For example, the

molecular simulation by Garde *et al.*¹¹⁴ reported a significant reduction of the crossover length scale from ~ 1 nm for pure water to the size of a small molecule on the addition of an ethanol like cosolvent to water. This is relevant in the present study as we consider here binary mixtures of water and glycerol (a polyol compound). Therefore, we presume a significant shortening of the small-to-large crossover distance to the size of a small solute, like methane, for the mixtures. Furthermore, a recent molecular simulation study¹¹⁸ further justifies our choice of the solute in the present study. The objective of the above study was to understand whether proteins behave like a small non-polar solute or a larger one. Quite surprisingly, the simulation has shown that proteins, having sizes of more than 1 nm, can behave as 'small' particles on the whole in terms of the hydrophobic effect. The above study also indicated that the proximity of polar and nonpolar residues of proteins makes the protein hydration structure very similar to that of a small nonpolar solute. Therefore, we expect that the key findings of the present work are well transferable to a more complex system with practical interest.

Conflicts of interest

There are no conflicts to declare.

Acknowledgements

VD acknowledges IIT Patna for a research fellowship. We acknowledge Dr Biman Jana for fruitful discussion. We acknowledge IIT Patna for computational support. This paper is dedicated to Sahitya, the newborn baby of the Daschakraborty family.

References

- 1 S. Izawa, M. Sato, K. Yokoigawa and Y. Inoue, Intracellular glycerol influences resistance to freeze stress in *Saccharomyces cerevisiae*: analysis of a quadruple mutant in glycerol dehydrogenase genes and glycerol-enriched cells, *Appl. Microbiol. Biotechnol.*, 2004, **66**, 108–114.
- 2 Y. Izumi, S. Sonoda, H. Yoshida, H. V. Danks and H. Tsumuki, Role of membrane transport of water and glycerol in the freeze tolerance of the rice stem borer, *Chilo suppressalis* Walker (Lepidoptera: Pyralidae), *J. Insect Physiol.*, 2006, **52**, 215–220.
- 3 J. R. Layne, Freeze tolerance and cryoprotectant mobilization in the gray treefrog (*Hyla versicolor*), *J. Exp. Zool.*, 1999, **283**, 221–225.
- 4 J. M. Lewis, K. V. Ewart and W. R. Driedzic, Freeze Resistance in Rainbow Smelt (*Osmerus mordax*): Seasonal Pattern of Glycerol and Antifreeze Protein Levels and Liver Enzyme Activity Associated with Glycerol Production, *Physiol. Biochem. Zool.*, 2004, **77**, 415–422.
- 5 P. H. Yancey, Organic osmolytes as compatible, metabolic and counteracting cytoprotectants in high osmolarity and other stresses, *J. Exp. Biol.*, 2005, **208**, 2819–2830.
- 6 S. Hohmann, Osmotic Stress Signaling and Osmoadaptation in Yeasts, *Microbiol. Mol. Biol. Rev.*, 2002, **66**, 300.
- 7 M. B. Burg and J. D. Ferraris, Intracellular Organic Osmolytes: Function and Regulation, *J. Biol. Chem.*, 2008, **283**, 7309–7313.
- 8 J. L. Dashnau, N. V. Nucci, K. A. Sharp and J. M. Vanderkooi, Hydrogen Bonding and the Cryoprotective Properties of Glycerol/Water Mixtures, *J. Phys. Chem. B*, 2006, **110**, 13670–13677.
- 9 J. J. Towey, A. K. Soper and L. Dougan, Low-Density Water Structure Observed in a Nanosegregated Cryoprotectant Solution at Low Temperatures from 285 to 238 K, *J. Phys. Chem. B*, 2016, **120**, 4439–4448.
- 10 J. J. Towey and L. Dougan, Structural Examination of the Impact of Glycerol on Water Structure, *J. Phys. Chem. B*, 2012, **116**, 1633–1641.
- 11 S. Daschakraborty, How do glycerol and dimethyl sulphoxide affect local tetrahedral structure of water around a nonpolar solute at low temperature? Importance of preferential interaction, *J. Chem. Phys.*, 2018, **148**, 134501.
- 12 C. Chen, W. Z. Li, Y. C. Song and J. Yang, Hydrogen Bonding Analysis of Glycerol Aqueous Solutions: A Molecular Dynamics Simulation Study, *J. Mol. Liq.*, 2009, **146**, 23.
- 13 L. D. Weng, C. Chen, J. G. Zuo and W. Z. Li, Molecular Dynamics Study of Effects of Temperature and Concentration on Hydrogen-Bond Abilities of Ethylene Glycol and Glycerol: Implications for Cryopreservation, *J. Phys. Chem. A*, 2011, **115**, 4729.
- 14 A. V. Egorov, A. P. Lyubartsev and A. Laaksonen, Molecular Dynamics Simulation Study of Glycerol+Water Liquid Mixtures, *J. Phys. Chem. B*, 2011, **115**, 14572–14581.
- 15 S. Indra and R. Biswas, How Heterogeneous Are Trehalose/Glycerol Cryoprotectant Mixtures? A Combined Time-Resolved Fluorescence and Computer Simulation Investigation, *J. Phys. Chem. B*, 2016, **120**, 11214–11228.
- 16 J. Jarabak, A. E. Seeds and P. Talalay, Reversible Cold Inactivation of a 17β -Hydroxysteroid Dehydrogenase of Human Placenta: Protective Effect of Glycerol*, *Biochemistry*, 1966, **5**, 1269–1279.
- 17 J. Jarabak, Human Placental 15-Hydroxyprostaglandin Dehydrogenase, *Proc. Natl. Acad. Sci. U. S. A.*, 1972, **69**, 533–536.
- 18 M. J. Ruwart and C. H. Suelter, Activation of Yeast Pyruvate Kinase by Natural and Artificial Cryoprotectants, *J. Biol. Chem.*, 1971, **246**, 5990–5993.
- 19 K. Gekko and S. N. Timasheff, Mechanism of protein stabilization by glycerol: preferential hydration in glycerol-water mixtures, *Biochemistry*, 1981, **20**, 4667–4676.
- 20 F.-G. Meng, Y.-K. Hong, H.-W. He, A. E. Lyubarev, B. I. Kurganov, Y.-B. Yan and H.-M. Zhou, Osmophobic effect of glycerol on irreversible thermal denaturation of rabbit creatine kinase, *Biophys. J.*, 2004, **87**, 2247–2254.
- 21 X. C. Tang and M. J. Pikal, The effect of stabilizers and denaturants on the cold denaturation temperatures of proteins and implications for freeze-drying, *Pharm. Res.*, 2005, **22**, 1167–1175.

- 22 S. Feng and Y.-B. Yan, Effects of glycerol on the compaction and stability of the wild type and mutated rabbit muscle creatine kinase, *Proteins*, 2008, **71**, 844–854.
- 23 K. Ruan, C. Xu, T. Li, J. Li, R. Lange and C. Balny, The thermodynamic analysis of protein stabilization by sucrose and glycerol against pressure-induced unfolding, *Eur. J. Biochem.*, 2003, **270**, 1654–1661.
- 24 A. Panuszko, P. Bruździak, E. Kaczkowska and J. Stangret, General Mechanism of Osmolytes' Influence on Protein Stability Irrespective of the Type of Osmolyte Cosolvent, *J. Phys. Chem. B*, 2016, **120**, 11159–11169.
- 25 F. Franks and R. Hatley, Stability of proteins at subzero temperatures: thermodynamics and some ecological consequences, *Pure Appl. Chem.*, 2009, **63**, 1367–1380.
- 26 D. Sanfelice and P. A. Temussi, Cold denaturation as a tool to measure protein stability, *Biophys. Chem.*, 2016, **208**, 4–8.
- 27 V. Vagenende, M. G. S. Yap and B. L. Trout, Mechanisms of Protein Stabilization and Prevention of Protein Aggregation by Glycerol, *Biochemistry*, 2009, **48**, 11084–11096.
- 28 G. Xie and S. N. Timasheff, The thermodynamic mechanism of protein stabilization by trehalose, *Biophys. Chem.*, 1997, **64**, 25–43.
- 29 T. O. Street, D. W. Bolen and G. D. Rose, A molecular mechanism for osmolyte-induced protein stability, *Proc. Natl. Acad. Sci. U. S. A.*, 2006, **103**, 13997–14002.
- 30 M. Pazhang, F. Mehrnejad, Y. Pazhang, H. Falahati and N. Chaparzadeh, Effect of sorbitol and glycerol on the stability of trypsin and difference between their stabilization effects in the various solvents, *Biotechnol. Appl. Biochem.*, 2016, **63**, 206–213.
- 31 I. Brovchenko, A. Krukau, N. Smolin, A. Oleinikova, A. Geiger and R. Winter, Thermal breaking of spanning water networks in the hydration shell of proteins, *J. Chem. Phys.*, 2005, **123**, 224905.
- 32 M. Koizumi, H. Hirai, T. Onai, K. Inoue and M. Hirai, Collapse of the hydration shell of a protein prior to thermal unfolding, *J. Appl. Crystallogr.*, 2007, **40**, s175–s178.
- 33 F. Mallamace, C. Corsaro, D. Mallamace, S. Vasi, C. Vasi, P. Baglioni, S. V. Buldyrev, S.-H. Chen and H. E. Stanley, Energy landscape in protein folding and unfolding, *Proc. Natl. Acad. Sci. U. S. A.*, 2016, **113**, 3159–3163.
- 34 A. Pica and G. Graziano, Shedding light on the extra thermal stability of thermophilic proteins, *Biopolymers*, 2016, **105**, 856–863.
- 35 S. Pal and S. Bandyopadhyay, Thermal unfolding of barstar and the properties of interfacial water around the unfolded forms, *J. Chem. Phys.*, 2013, **139**, 235101.
- 36 A. L. Jonsson, K. A. Scott and V. Daggett, Dynamomechanics: A Consensus View of the Protein Unfolding/Folding Transition State Ensemble across a Diverse Set of Protein Folds, *Biophys. J.*, 2009, **97**, 2958–2966.
- 37 M. S. Li, D. K. Klimov and D. Thirumalai, Finite Size Effects on Thermal Denaturation of Globular Proteins, *Phys. Rev. Lett.*, 2004, **93**, 268107.
- 38 R. Ghosh, S. Roy and B. Bagchi, Solvent Sensitivity of Protein Unfolding: Dynamical Study of Chicken Villin Headpiece Subdomain in Water–Ethanol Binary Mixture, *J. Phys. Chem. B*, 2013, **117**, 15625–15638.
- 39 P. Chatterjee and N. Sengupta, Signatures of protein thermal denaturation and local hydrophobicity in domain specific hydration behavior: a comparative molecular dynamics study, *Mol. BioSyst.*, 2016, **12**, 1139–1150.
- 40 D. Sanfelice, E. Morandi, A. Pastore, N. Niccolai and P. A. Temussi, Cold Denaturation Unveiled: Molecular Mechanism of the Asymmetric Unfolding of Yeast Frataxin, *ChemPhysChem*, 2015, **16**, 3599–3602.
- 41 P. L. Privalov, Cold denaturation of proteins, *Crit. Rev. Biochem. Mol. Biol.*, 1990, **25**, 281–305.
- 42 A. Pastore, S. R. Martin, A. Politou, K. C. Kondapalli, T. Stemmler and P. A. Temussi, Unbiased Cold Denaturation: Low- and High-Temperature Unfolding of Yeast Frataxin under Physiological Conditions, *J. Am. Chem. Soc.*, 2007, **129**, 5374–5375.
- 43 V. R. Agashe and J. B. Udgaonkar, Thermodynamics of Denaturation of Barstar: Evidence for Cold Denaturation and Evaluation of the Interaction with Guanidine Hydrochloride, *Biochemistry*, 1995, **34**, 3286–3299.
- 44 P. L. Privalov, Y. V. Griko, S. Y. Venyaminov and V. P. Kutysenko, Cold denaturation of myoglobin, *J. Mol. Biol.*, 1986, **190**, 487–498.
- 45 C. Yang, S. Jang and Y. Pak, A fully atomistic computer simulation study of cold denaturation of a β -hairpin, *Nat. Commun.*, 2014, **5**, 5773.
- 46 C. L. Dias, T. Ala-Nissila, J. Wong-ekkabut, I. Vattulainen, M. Grant and M. Karttunen, The hydrophobic effect and its role in cold denaturation, *Cryobiology*, 2010, **60**, 91–99.
- 47 C. L. Dias, T. Ala-Nissila, M. Karttunen, I. Vattulainen and M. Grant, Microscopic Mechanism for Cold Denaturation, *Phys. Rev. Lett.*, 2008, **100**, 118101.
- 48 F. Franks, Protein destabilization at low temperatures, *Adv. Protein Chem.*, 1995, **46**, 105–139.
- 49 C.-J. Tsai, J. V. J. Maizel and R. Nussinov, The hydrophobic effect: a new insight from cold denaturation and a two-state water structure, *Crit. Rev. Biochem. Mol. Biol.*, 2002, **37**, 55–69.
- 50 C. F. Lopez, R. K. Darst and P. J. Rossky, Mechanistic Elements of Protein Cold Denaturation, *J. Phys. Chem. B*, 2008, **112**, 5961–5967.
- 51 C. Camilloni, D. Bonetti, A. Morrone, R. Giri, C. M. Dobson, M. Brunori, S. Gianni and M. Vendruscolo, Towards a structural biology of the hydrophobic effect in protein folding, *Sci. Rep.*, 2016, **6**, 28285.
- 52 M. Maiti, S. Weiner, S. V. Buldyrev, H. E. Stanley and S. Sastry, Potential of mean force between hydrophobic solutes in the Jagla model of water and implications for cold denaturation of proteins, *J. Chem. Phys.*, 2012, **136**, 044512.
- 53 S. Parui and B. Jana, Pairwise Hydrophobicity at Low Temperature: Appearance of a Stable Second Solvent-Separated Minimum with Possible Implication in Cold Denaturation, *J. Phys. Chem. B*, 2017, **121**, 7016–7026.
- 54 Y. Li, B. Shan and D. P. Raleigh, The cold denatured state is compact but expands at low temperatures: hydrodynamic

- properties of the cold denatured state of the C-terminal domain of L9, *J. Mol. Biol.*, 2007, **368**, 256–262.
- 55 G. Graziano, On the molecular origin of cold denaturation of globular proteins, *Phys. Chem. Chem. Phys.*, 2010, **12**, 14245–14252.
- 56 M. L. Romero-Romero, A. Inglés-Prieto, B. Ibarra-Molero and J. M. Sanchez-Ruiz, Highly Anomalous Energetics of Protein Cold Denaturation Linked to Folding-Unfolding Kinetics, *PLoS One*, 2011, **6**, e23050.
- 57 S. Parui and B. Jana, Molecular Insights into the Unusual Structure of an Antifreeze Protein with a Hydrated Core, *J. Phys. Chem. B*, 2018, **122**, 9827–9839.
- 58 S. B. Kim, J. C. Palmer and P. G. Debenedetti, Computational investigation of cold denaturation in the Trp-cage miniprotein, *Proc. Natl. Acad. Sci. U. S. A.*, 2016, **113**, 8991–8996.
- 59 A. Ben-Naim, Theory of Cold Denaturation of Proteins, *Adv. Biol. Chem.*, 2013, **3**, 29–39.
- 60 V. Bianco and G. Franzese, Contribution of Water to Pressure and Cold Denaturation of Proteins, *Phys. Rev. Lett.*, 2015, **115**, 108101.
- 61 S. Paul and S. Paul, The influence of trehalose on hydrophobic interactions of small nonpolar solute: a molecular dynamics simulation study, *J. Chem. Phys.*, 2013, **139**, 044508.
- 62 S. Paul and S. Paul, Effects of the temperature and trehalose concentration on the hydrophobic interactions of a small nonpolar neopentane solute: a molecular dynamics simulation study, *RSC Adv.*, 2014, **4**, 34267.
- 63 Z. Su, G. Ravindhran and C. L. Dias, Effects of Trimethylamine-*N*-oxide (TMAO) on Hydrophobic and Charged Interactions, *J. Phys. Chem. B*, 2018, **122**, 5557–5566.
- 64 M. V. Athawale, J. S. Dordick and S. Garde, Osmolyte Trimethylamine-*N*-Oxide Does Not Affect the Strength of Hydrophobic Interactions: Origin of Osmolyte Compatibility, *Biophys. J.*, 2005, **89**, 858–866.
- 65 M. Mukherjee and J. Mondal, Heterogeneous Impacts of Protein-Stabilizing Osmolytes on Hydrophobic Interaction, *J. Phys. Chem. B*, 2018, **122**, 6922–6930.
- 66 R. Sarma and S. Paul, Hydrophobic interactions in presence of osmolytes urea and trimethylamine-*N*-oxide, *J. Chem. Phys.*, 2011, **135**, 174501.
- 67 N. F. A. van der Vegt and D. Nayar, The Hydrophobic Effect and the Role of Cosolvents, *J. Phys. Chem. B*, 2017, **121**, 9986–9998.
- 68 S. Murakami, T. Hayashi and M. Kinoshita, Effects of salt or cosolvent addition on solubility of a hydrophobic solute in water: Relevance to those on thermal stability of a protein, *J. Chem. Phys.*, 2017, **146**, 055102.
- 69 M. Janado and T. Nishida, Effect of sugars on the solubility of hydrophobic solutes in water, *J. Solution Chem.*, 1981, **10**, 489–500.
- 70 S. Banerjee, S. Roy and B. Bagchi, Enhanced Pair Hydrophobicity in the Water–Dimethylsulfoxide (DMSO) Binary Mixture at Low DMSO Concentrations, *J. Phys. Chem. B*, 2010, **114**, 12875–12882.
- 71 R. Halder and B. Jana, Unravelling the Composition-Dependent Anomalies of Pair Hydrophobicity in Water-Ethanol Binary Mixtures, *J. Phys. Chem. B*, 2018, **122**, 6801–6809.
- 72 Z. Su, F. Mahmoudinobar and C. L. Dias, Effects of Trimethylamine-*N*-oxide on the Conformation of Peptides and its Implications for Proteins, *Phys. Rev. Lett.*, 2017, **119**, 108102.
- 73 D. Van Der Spoel, E. Lindahl, B. Hess, G. Groenhof, A. E. Mark and H. J. C. Berendsen, GROMACS: fast, flexible, and free, *J. Comput. Chem.*, 2005, **26**, 1701–1718.
- 74 L. B. Lane, Freezing Points of Glycerol and Its Aqueous Solutions, *Ind. Eng. Chem.*, 1925, **17**, 924.
- 75 R. Chelli, P. Procacci, G. Cardini, R. G. Della Valle and S. Califano, Glycerol condensed phases Part I. A molecular dynamics study, *Phys. Chem. Chem. Phys.*, 1999, **1**, 871–877.
- 76 J. Blicek, F. Affouard, P. Bordat, A. Lerbret and M. Descamps, Molecular dynamics simulations of glycerol glass-forming liquid, *Chem. Phys.*, 2005, **317**, 253–257.
- 77 J. L. F. Abascal and C. Vega, A general purpose model for the condensed phases of water: TIP4P/2005, *J. Chem. Phys.*, 2005, **123**, 234505.
- 78 F. O. Akinkunmi, D. A. Jahn and N. Giovambattista, Effects of Temperature on the Thermodynamic and Dynamical Properties of Glycerol–Water Mixtures: A Computer Simulation Study of Three Different Force Fields, *J. Phys. Chem. B*, 2015, **119**, 6250–6261.
- 79 W. L. Jorgensen, D. S. Maxwell and J. Tirado-Rives, Development and Testing of the OPLS All-Atom Force Field on Conformational Energetics and Properties of Organic Liquids, *J. Am. Chem. Soc.*, 1996, **118**, 11225–11236.
- 80 S. Nosé, A unified formulation of the constant temperature molecular dynamics methods, *J. Chem. Phys.*, 1984, **81**, 511–519.
- 81 W. G. Hoover, Canonical dynamics: Equilibrium phase-space distributions, *Phys. Rev. A: At., Mol., Opt. Phys.*, 1985, **31**, 1695–1697.
- 82 M. Parrinello and A. Rahman, Polymorphic transitions in single crystals: A new molecular dynamics method, *J. Appl. Phys.*, 1981, **52**, 7182–7190.
- 83 G. M. Torrie and J. P. Valleau, Nonphysical sampling distributions in Monte Carlo free-energy estimation: Umbrella sampling, *J. Comput. Phys.*, 1977, **23**, 187–199.
- 84 S. Kumar, J. M. Rosenberg, D. Bouzida, R. H. Swendsen and P. A. Kollman, THE weighted histogram analysis method for free-energy calculations on biomolecules. I. The method, *J. Comput. Chem.*, 1992, **13**, 1011–1021.
- 85 B. M. Pettitt and P. J. Rossky, Alkali halides in water: ion–solvent correlations and ion–ion potentials of mean force at infinite dilution, *J. Chem. Phys.*, 1986, **84**, 5836–5844.
- 86 N. Choudhury and B. M. Pettitt, Enthalpy–Entropy Contributions to the Potential of Mean Force of Nanoscopic Hydrophobic Solutes, *J. Phys. Chem. B*, 2006, **110**, 8459–8463.
- 87 N. Choudhury and B. M. Pettitt, On the Mechanism of Hydrophobic Association of Nanoscopic Solutes, *J. Am. Chem. Soc.*, 2005, **127**, 3556–3567.
- 88 S. Ou, S. Patel and B. A. Bauer, Free Energetics of Carbon Nanotube Association in Pure and Aqueous Ionic Solutions, *J. Phys. Chem. B*, 2012, **116**, 8154–8168.

- 89 D. E. Smith and A. D. J. Haymet, Free energy, entropy, and internal energy of hydrophobic interactions: Computer simulations, *J. Chem. Phys.*, 1993, **98**, 6445–6454.
- 90 S. W. Rick, Increasing the Efficiency of Free Energy Calculations Using Parallel Tempering and Histogram Reweighting, *J. Chem. Theory Comput.*, 2006, **2**, 939–946.
- 91 S. Jo, C. Chipot and B. Roux, Efficient Determination of Relative Entropy Using Combined Temperature and Hamiltonian Replica-Exchange Molecular Dynamics, *J. Chem. Theory Comput.*, 2015, **11**, 2234–2244.
- 92 T. Ghosh, A. E. García and S. Garde, Molecular Dynamics Simulations of Pressure Effects on Hydrophobic Interactions, *J. Am. Chem. Soc.*, 2001, **123**, 10997–11003.
- 93 S. Shimizu and H. S. Chan, Temperature dependence of hydrophobic interactions: A mean force perspective, effects of water density, and nonadditivity of thermodynamic signatures, *J. Chem. Phys.*, 2000, **113**, 4683–4700.
- 94 C. L. Dias, T. Hynninen, T. Ala-Nissila, A. S. Foster and M. Karttunen, Hydrophobicity within the three-dimensional Mercedes-Benz model: potential of mean force, *J. Chem. Phys.*, 2011, **134**, 065106.
- 95 J.-L. Li, R. Car, C. Tang and N. S. Wingreen, Hydrophobic interaction and hydrogen-bond network for a methane pair in liquid water, *Proc. Natl. Acad. Sci. U. S. A.*, 2007, **104**, 2626–2630.
- 96 D. E. Smith, L. Zhang and A. D. J. Haymet, Entropy of association of methane in water: a new molecular dynamics computer simulation, *J. Am. Chem. Soc.*, 1992, **114**, 5875–5876.
- 97 L. X. Dang, Potential of mean force for the methane-methane pair in water, *J. Chem. Phys.*, 1994, **100**, 9032–9034.
- 98 R. Zangi, Can Salting-In/Salting-Out Ions be Classified as Chaotropes/Kosmotropes?, *J. Phys. Chem. B*, 2010, **114**, 643–650.
- 99 H. S. Frank and M. W. Evans, Free Volume and Entropy in Condensed Systems III. Entropy in Binary Liquid Mixtures; Partial Molal Entropy in Dilute Solutions; Structure and Thermodynamics in Aqueous Electrolytes, *J. Chem. Phys.*, 1945, **13**, 507–532.
- 100 W. Kauzmann, Some factors in the interpretation of protein denaturation, *Adv. Protein Chem.*, 1959, **14**, 1–63.
- 101 R. Haselmeier, M. Holz, W. Marbach and H. Weingaertner, Water Dynamics near a Dissolved Noble Gas. First Direct Experimental Evidence for a Retardation Effect, *J. Phys. Chem.*, 1995, **99**, 2243–2246.
- 102 N. Muller, Search for a realistic view of hydrophobic effects, *Acc. Chem. Res.*, 1990, **23**, 23–28.
- 103 G. Némethy and H. A. Scheraga, Structure of Water and Hydrophobic Bonding in Proteins. II. Model for the Thermodynamic Properties of Aqueous Solutions of Hydrocarbons, *J. Chem. Phys.*, 1962, **36**, 3401–3417.
- 104 N. Galamba, Water's Structure around Hydrophobic Solutes and the Iceberg Model, *J. Phys. Chem. B*, 2013, **117**, 2153–2159.
- 105 N. Galamba, Water Tetrahedrons, Hydrogen-Bond Dynamics, and the Orientational Mobility of Water around Hydrophobic Solutes, *J. Phys. Chem. B*, 2014, **118**, 4169–4176.
- 106 N. Galamba, On the Effects of Temperature, Pressure, and Dissolved Salts on the Hydrogen-Bond Network of Water, *J. Phys. Chem. B*, 2013, **117**, 589–601.
- 107 J. Grdadolnika, F. Merzela and F. Avbelj, Origin of hydrophobicity and enhanced water hydrogen bond strength near purely hydrophobic solutes, *Proc. Natl. Acad. Sci. U. S. A.*, 2017, **114**, 322–327.
- 108 C. A. Koh, R. P. Wisbey, X. P. Wu, R. E. Westacott and A. K. Soper, Water ordering around methane during hydrate formation, *J. Chem. Phys.*, 2000, **113**, 6390–6397.
- 109 P.-L. Chau and A. J. Hardwick, A new order parameter for tetrahedral configurations, *Mol. Phys.*, 1998, **93**, 511–518.
- 110 J. R. Errington and P. G. Debenedetti, Relationship between Structural Order and the Anomalies of Liquid Water, *Nature*, 2001, **409**, 318–321.
- 111 K. Lum, D. Chandler and J. D. Weeks, Hydrophobicity at Small and Large Length Scales, *J. Phys. Chem. B*, 1999, **103**, 4570–4577.
- 112 D. M. Huang and D. Chandler, Temperature and length scale dependence of hydrophobic effects and their possible implications for protein folding, *Proc. Natl. Acad. Sci. U. S. A.*, 2000, **97**, 8324–8327.
- 113 H. S. Ashbaugh and M. E. Paulaitis, Effect of Solute Size and Solute–Water Attractive Interactions on Hydration Water Structure around Hydrophobic Solutes, *J. Am. Chem. Soc.*, 2001, **123**, 10721–10728.
- 114 S. Rajamani, T. M. Truskett and S. Garde, Hydrophobic hydration from small to large lengthscales: Understanding and manipulating the crossover, *Proc. Natl. Acad. Sci. U. S. A.*, 2005, **102**, 9475.
- 115 H. S. Ashbaugh and L. R. Pratt, Colloquium: Scaled particle theory and the length scales of hydrophobicity, *Rev. Mod. Phys.*, 2006, **78**, 159–178.
- 116 S. Garde and A. J. Patel, Unraveling the hydrophobic effect, one molecule at a time, *Proc. Natl. Acad. Sci. U. S. A.*, 2011, **108**, 16491.
- 117 R. Zangi, Driving Force for Hydrophobic Interaction at Different Length Scales, *J. Phys. Chem. B*, 2011, **115**, 2303–2311.
- 118 C. Camilloni, D. Bonetti, A. Morrone, R. Giri, C. M. Dobson, M. Brunori, S. Gianni and M. Vendruscolo, Towards a structural biology of the hydrophobic effect in protein folding, *Sci. Rep.*, 2016, **6**, 28285.